

# Quantitative wave-particle duality in uniform multipath interferometers with symmetric which-path detector states

L. F. Melo,<sup>1,2</sup> O. Jiménez,<sup>3</sup> and L. Neves<sup>1</sup>

<sup>1</sup>Departamento de Física, Universidade Federal de Minas Gerais, Belo Horizonte, MG, Brazil

<sup>2</sup>QUIIN - Quantum Industrial Innovation, Centro de Competência Embrapii Cimatec, SENAI CIMATEC, Av. Orlando Gomes, 1845, Salvador, BA, 41850-010, Brazil

<sup>3</sup>Centro Multidisciplinario de Física, Vicerrectoría de Investigación, Universidad Mayor, Santiago 8580745, Chile

(Dated: January 21, 2026)

A quantum system (*quanton*) traverses an interferometer with  $N$  equally probable paths and interacts with another quantum system (*detector*) that stores path information in a set of symmetric states. In this interferometric framework, we present entropic wave-particle duality relations between quantum coherence, characterized by the relative entropy of coherence of the quanton state, and which-path knowledge, quantified by the mutual information obtained through detector-state discrimination. By applying a general optimal discrimination measurement, which has a closed-form solution and encompasses other fundamental strategies as special cases, we provide an exact quantification of which-path knowledge in a variety of scenarios. This measurement is carried out in two steps. First, an optimal separation map with a prescribed separation level  $\xi \in [0, 1]$  probabilistically reduces the overlaps between the input detector states with maximum success rate, or increases them in case of failure. Then, a minimum-error (ME) measurement discriminates either only the successful outputs (standard approach) or both the successful and failure outputs (concatenated approach). We show that the duality relation is tighter at  $\xi = 0$ , where both approaches reduce to the ME measurement. For  $\xi > 0$ , each approach yields a distinct relation that becomes less tight as  $\xi$  increases, with the concatenated one providing the tighter bound. Finally, by using the discrete uncertainty principle, we determine the sets of detector states that lead to saturation of the duality relation, showing that they span  $n$ -dimensional subspaces of the detector space, where  $n$  divides  $N$ . As a result, nontrivial saturation occurs only for interferometers with a nonprime number of paths. From the identified saturating sets, we highlight how the quanton-detector correlations underlie this phenomenon.

## I. INTRODUCTION

Wave-particle duality relations are quantitative statements on the trade-off between the “strength” of interference effects produced by individual quantum systems (quantons) in an interferometer and the knowledge of which path they took inside it [1–10]. The first explicit relation of this type is due to Greenberger and YaSin [5], who considered two-path interferometers in which the wavelike behavior is quantified by the *a priori* fringe visibility ( $\mathcal{V}_0$ ) and the particlelike behavior by the path predictability ( $\mathcal{P}$ ), leading to the trade-off

$$\mathcal{V}_0^2 + \mathcal{P}^2 \leq 1. \quad (1)$$

The path information is obtained predictively by using prior knowledge of the probabilities for the quanton to take each arm and betting on the most likely one. In addition, prior knowledge of the quanton state in the path basis allows one to estimate, *a priori*, the fringe visibility of the interference pattern that will emerge.

The essence of the discussion on wave-particle duality, as conceived in Einstein’s recoiling-slit proposal to challenge Bohr’s complementarity principle [11], relied on actively intervening in the experiment to obtain path information. Thus, the framework considered by Greenberger and YaSin [5], based solely on predictive analysis using *a priori* information, was unable to capture this aspect adequately. In contrast, Englert’s [8] fully quantum-mechanical approach established a retrodictive framework that embodied the original concept of duality. He considered two-path interferometers, inside which the quanton is unitarily coupled to an auxiliary quantum system. As a result, the ancilla stores path information in

its states, thereby functioning as a which-path detector. The amount of information that becomes available in this process is quantified by the distinguishability ( $\mathcal{D}$ ) of the detector states and can be extracted retrodictively by an optimal measurement that discriminates between them. (Note that a nonoptimal measurement can only extract part of this information.) Due to the quanton-detector coupling, the resulting interference pattern exhibits a reduced fringe visibility ( $\mathcal{V}$ ) compared to the *a priori* value, i.e.,  $\mathcal{V} < \mathcal{V}_0$ . In this retrodictive framework, Englert [8] showed that the trade-off between the *a posteriori* quantifiers of wavelike and particlelike behaviors is

$$\mathcal{V}^2 + \mathcal{D}^2 \leq 1. \quad (2)$$

Although derived in different frameworks, the duality relations in Eqs. (1) and (2) share the same structure: full wavelike behavior ( $\mathcal{V}_0$  or  $\mathcal{V} = 1$ ) precludes particlelike behavior ( $\mathcal{P}$  or  $\mathcal{D} = 0$ ), and vice versa, while also allowing for intermediate cases with partial contributions from both.

Once well established in the two-path case, the next step was to generalize these duality relations to interferometers with more than two paths. In this scenario, the inherent greater complexity of characterizing wavelike and particlelike behaviors—associated with the larger number of parameters involved—has led to several generalizations of both relations in Eqs. (1) and (2) [12–23]. Within the retrodictive framework, where the present work is situated, we consider the approaches introduced by Bera *et al.* [16] and Bagan *et al.* [17], who derived duality relations between quantum coherence and which-path knowledge. In these generalizations, the coherence of the quanton state in the path basis characterizes the wavelike behavior, and is quantified by suitable measures such

as the  $l_1$ -norm or the relative entropy of coherence [24]. Conversely, which-path knowledge characterizes particlelike behavior, and is quantified by the success probability (or mutual information) associated with detector-state discrimination.

When the detector states are not orthogonal, perfect discrimination is impossible; nevertheless, several strategies can optimize the process according to preestablished criteria [25–27]. If the chosen strategy extracts all available path information, which-path knowledge coincides with distinguishability; otherwise, it is strictly smaller. In general, the discrimination strategies lead to correct, erroneous, or inconclusive outcomes, and can be formulated as optimization problems where the error rate is minimized subject to a fixed inconclusive rate [28–30]. In this context, Bera *et al.* [16] employed the discrimination of the detector states with zero error rate (which led to a critical inconclusive rate). On the other hand, Bagan *et al.* [17] adopted the discrimination with zero inconclusive rate, the same criterion underlying Englert's derivation of the duality relation in Eq. (2). More recently, Bagan *et al.* [21] extended their previous analysis by considering a strategy that allows both error and inconclusive rates to be nonzero. In all these cases [16, 17, 21], due to the lack of a general solution for the state discrimination problem, the authors consider only upper bounds for which-path knowledge. As a result, this quantity is generally overestimated, which prevents a clear assessment of the true saturation of the duality relations and hinders a more precise understanding of the quanton-detector correlations.

Here, we overcome this limitation by introducing an interferometric framework that enables the exact quantification of which-path knowledge across a variety of scenarios, including those studied in Refs. [16, 17, 21] and extending beyond them. We consider a quanton traversing an interferometer with  $N$  equally probable paths (uniform interferometer) and interacting with a detector that stores path information in a set of symmetric states. Under these conditions, the detector states can be discriminated through a general optimal measurement, which has a closed-form solution and encompasses other fundamental strategies as special cases. This measurement is carried out in two steps. First, an optimal separation map [31] with a prescribed separation level  $\xi \in [0, 1]$  probabilistically reduces the overlaps between the input detector states with maximum success rate, or increases them in case of failure. Then, a minimum-error measurement discriminates either only the successful outputs (standard approach) or both the successful and failure outputs (concatenated approach). In this interferometric framework, we establish entropic wave-particle duality relations between quantum coherence and which-path knowledge, quantified respectively by the relative entropy of coherence of the quanton state and the mutual information from the detector-state discrimination. We show that the relation is tighter at  $\xi = 0$ , where both the standard and concatenated approaches reduce to the minimum-error measurement. For  $\xi > 0$ , each approach yields a distinct relation that becomes less tight as  $\xi$  increases, with the concatenated one providing the tighter bound. Finally, by employing the discrete uncertainty principle [32], we identify the sets of detector states that lead to saturation of the

duality relation, showing that they span  $n$ -dimensional subspaces of the detector space, where  $n$  divides  $N$ . In this case, saturation beyond the trivial limits of full wavelike or particlelike behaviors occurs only for interferometers with a non-prime number of paths. From the identified saturating sets, we highlight how the quanton-detector correlations underlie this phenomenon.

The paper is organized as follows. In Sec. II, we introduce the elements for a quantitative study of wave-particle duality within our interferometric framework. In Sec. III, we derive the duality relations under different measurement strategies for obtaining path information, and assess their behavior via numerical simulations in Sec. IV. The conditions for saturation of the duality relation are analyzed in Sec. V, and we present our concluding remarks in Sec. VI.

## II. INTERFEROMETRIC FRAMEWORK

In this section, we introduce the interferometric framework, the entropic measures of wavelike and particlelike properties, and the measurement strategies for acquiring which-path knowledge. Together, these elements form the basis for our analysis of wave-particle duality in the subsequent sections.

### A. Uniform $N$ -path interferometers with symmetric which-path detector states

Consider a quanton that, upon entering an  $N$ -path interferometer, is prepared in the superposition state

$$|\psi\rangle_q = \frac{1}{\sqrt{N}} \sum_{\ell=0}^{N-1} |\ell\rangle_q, \quad (3)$$

where  $\{|\ell\rangle_q\}_{\ell=0}^{N-1}$  denotes the orthonormal basis associated with the  $N$  possible paths. Since each path is taken with equal probability  $1/N$ , we refer to this interferometer as *uniform*.

Inside the interferometer, the quanton interacts with an auxiliary quantum system in an  $N$ -dimensional Hilbert space, which is assumed to be initially in a fixed pure state given by

$$|\alpha_0\rangle_d = \sum_{k \in \mathcal{I}} a_k |k\rangle_d, \quad (4)$$

where  $\mathcal{I} \subseteq \{0, \dots, N-1\}$  denotes the support of  $|\alpha_0\rangle_d$  in the orthonormal basis  $\{|k\rangle_d\}_{k=0}^{N-1}$ , with  $|\mathcal{I}| = n \leq N$ ; the coefficients  $a_k \in \mathbb{R}$  are strictly positive for all  $k \in \mathcal{I}$ , and satisfy  $\sum_{k \in \mathcal{I}} a_k^2 = 1$ . The interaction is implemented through the controlled unitary operation

$$\hat{U}_{qd} = \sum_{\ell=0}^{N-1} |\ell\rangle_q \langle \ell| \otimes \hat{V}_d^{\ell}, \quad (5)$$

where

$$\hat{V}_d = \sum_{k \in \mathcal{I}} \omega^k |k\rangle_d \langle k|, \quad (6)$$

with  $\omega = \exp(2\pi i/N)$ . Thus, the initial bipartite state  $|\psi\rangle_q|\alpha_0\rangle_d$  evolves into

$$|\Psi\rangle = \frac{1}{\sqrt{N}} \sum_{\ell=0}^{N-1} |\ell\rangle_q |\alpha_\ell\rangle_d, \quad (7)$$

where

$$|\alpha_\ell\rangle_d = \sum_{k \in \mathcal{I}} a_k \omega^{k\ell} |k\rangle_d \quad (8)$$

are *symmetric* states under the action of  $\hat{V}$ , as they satisfy  $|\alpha_\ell\rangle = \hat{V}|\alpha_{\ell-1}\rangle = \hat{V}^\ell|\alpha_0\rangle$  and  $|\alpha_0\rangle = \hat{V}|\alpha_{N-1}\rangle$  [33, 34]. Clearly, the correlation established by the interaction encodes information about the quanton's path in the state of the auxiliary system, which thereby acts as a which-path detector.

## B. Characterizing wavelike properties

Recent approaches to wave-particle duality relations in multipath interferometers show that quantum coherence not only quantifies, but also offers a clear and intuitive picture of the quanton's wavelike behavior [16–18, 21]. In this context, an entropic quantifier of this property is the relative entropy of coherence, which, for a given state  $\hat{\rho}$ , is defined as [24]

$$C_r(\hat{\rho}) = S(\hat{\rho}_{\text{diag}}) - S(\hat{\rho}), \quad (9)$$

where  $S(\hat{\rho}) = -\text{Tr}(\hat{\rho} \log_2 \hat{\rho})$  is the von Neumann entropy and  $\hat{\rho}_{\text{diag}}$  denotes the diagonal part of  $\hat{\rho}$  with respect to a reference orthonormal basis.

In the path basis, the *a priori* coherence,  $C_{r0}$ , of the quanton state  $|\psi\rangle_q$  in Eq. (3) is

$$C_{r0}(|\psi\rangle_q\langle\psi|) = \log_2 N, \quad (10)$$

which is the maximum value, as expected for a uniform  $N$ -path interferometer.

After the quanton-detector interaction, the reduced state of each subsystem is obtained from Eq. (7) by tracing out the other, i.e.,  $\hat{\rho}_q = \text{Tr}_d|\Psi\rangle\langle\Psi|$  and  $\hat{\rho}_d = \text{Tr}_q|\Psi\rangle\langle\Psi|$ . In particular, the reduced state of the detector is given by

$$\hat{\rho}_d = \frac{1}{N} \sum_{\ell=0}^{N-1} |\alpha_\ell\rangle_d\langle\alpha_\ell| = \sum_{k \in \mathcal{I}} a_k^2 |k\rangle_d\langle k|, \quad (11)$$

where we used Eq. (8) and the fact that  $\omega$  is a primitive  $N$ th root of unity, which satisfies the orthogonality relation  $\sum_{\ell=0}^{N-1} \omega^{\ell(k-k')} = N\delta_{kk'}$ . Since  $\hat{\rho}_q$  and  $\hat{\rho}_d$  are the reduced states of a global pure state, it follows that  $S(\hat{\rho}_q) = S(\hat{\rho}_d)$ . Therefore, as  $[\hat{\rho}_q]_{\text{diag}} = \frac{1}{N} \sum_{\ell} |\ell\rangle_q\langle\ell|$ , the *a posteriori* coherence of the quanton state is

$$C_r(\hat{\rho}_q) = \log_2 N - H(\{a_k^2\}), \quad (12)$$

where  $H(\{a_k^2\})$  denotes the Shannon entropy of the probability distribution  $\{a_k^2\}$ .

The effective measure we adopt to characterize the quanton's wavelike properties is the normalized version of the coherence in Eq. (12), given by

$$\mathcal{C} = \frac{C_r(\hat{\rho}_q)}{\log_2 N} = 1 - \frac{H(\{a_k^2\})}{\log_2 N}, \quad (13)$$

which satisfies  $0 \leq \mathcal{C} \leq 1$ . For simplicity, we refer to this normalized quantity as coherence. Note that  $\mathcal{C} \leq 1$ , with equality holding if and only if  $|\alpha_\ell\rangle_d = |\alpha_0\rangle_d$  for all  $\ell$ . Thus, the process of encoding path information into the detector states inevitably reduces the *a priori* coherence. In particular, when these states are mutually orthogonal, we have  $H(\{a_k^2\}) = \log_2 N$ . In this case,  $\mathcal{C} = 0$ , implying that no interference effects can arise due to the availability of full which-path information in the detector states.

## C. Characterizing particlelike properties

As described above, the coupling with the quanton stores which-path information in the detector. To gain knowledge about the quanton's path, one must perform a measurement that discriminates the detector states, noting that not all measurements can extract all the available information. In this context, following Refs. [17, 21], we characterize the particlelike properties of the quanton by the mutual information between the detector states and the outcomes of a measurement designed to discriminate them.

Let  $D$  and  $M$  be the random variables associated with the detector states and the measurement outcomes, respectively. We can express the mutual information between them as

$$I(M : D) = H(D) - H(D|M), \quad (14)$$

where  $H(D|M)$  denotes the conditional entropy of  $D$  given  $M$ . The variable  $D$  takes values in the set  $\{\ell\}_{\ell=0}^{N-1}$ , corresponding to the state  $|\alpha_\ell\rangle_d$ , with probability  $1/N$ ; hence,  $H(D) = \log_2 N$ . On the other hand,  $M$  takes values in the set  $\{j\}_{j=0}^{N'-1}$ , corresponding to the probabilities  $p_j = \text{Tr}(\hat{\Pi}_j \hat{\rho}_d)$  of a given  $N'$ -outcome positive operator-valued measure (POVM)  $\mathbf{\Pi} = \{\hat{\Pi}_j \mid \hat{\Pi}_j \geq 0, \sum_{j=0}^{N'-1} \hat{\Pi}_j = \hat{I}\}$  performed on the detector. Thus, the conditional entropy can be written as

$$H(D|M) = \sum_{j=0}^{N'-1} p_j H(\{p_{\ell|j}\}), \quad (15)$$

where

$$p_{\ell|j} \equiv p(\alpha_\ell|j) = \frac{d\langle\alpha_\ell|\hat{\Pi}_j|\alpha_\ell\rangle_d}{N \text{Tr}(\hat{\Pi}_j \hat{\rho}_d)} \quad (16)$$

is the probability that the detector state was  $|\alpha_\ell\rangle_d$ , given that the outcome  $j$  was obtained. The expression for this conditional probability follows from Bayes' rule.

Similarly to coherence, we define the normalized mutual information as a measure of the quanton's particlelike behavior,

given by

$$\mathcal{K}(\mathbf{\Pi}) = \frac{I(M : D)}{\log_2 N} = 1 - \sum_{j=0}^{N'-1} p_j \frac{H(\{p_{\ell|j}\})}{\log_2 N}, \quad (17)$$

which satisfies  $0 \leq \mathcal{K}(\mathbf{\Pi}) \leq 1$ . The notation  $\mathcal{K}(\mathbf{\Pi})$  highlights that this quantity—which we refer to as *which-path knowledge* [9, 10]—depends on the specific discrimination strategy applied, expressed by the second term on the right-hand side of Eq. (17). When the measurement is able to extract all the available information stored in the detector states,  $\mathcal{K}(\mathbf{\Pi})$  reaches its maximum value:

$$\mathcal{K}_{\max} = \max_{\mathbf{\Pi}} \mathcal{K}(\mathbf{\Pi}). \quad (18)$$

The maximum mutual information over all POVMs is known as the *accessible information*, and in the context of wave-particle duality relations, it quantifies path *distinguishability* [8, 17]. Except for a few special cases, there is no general analytical solution to the problem of maximizing the mutual information. As a result, when deriving duality relations in multipath interferometers, one is typically restricted to providing bounds for the which-path knowledge [16–18, 21]. Otherwise, when an analytical solution is unavailable, exact expressions for  $\mathcal{K}(\mathbf{\Pi})$  ( $\leq \mathcal{K}_{\max}$ ) can still be obtained by adopting physically motivated strategies for discriminating the detector states, which is the approach we follow.

#### D. Strategies for which-path state discrimination

Within the framework outlined above, the uniformity of the interferometer implies that acquiring which-path knowledge amounts to discriminating among  $N$  symmetric,  $n$ -dimensional pure states ( $N \geq n \geq 2$ ), each prepared with equal *a priori* probability  $1/N$ . For this family of states, although the solution that yields  $\mathcal{K}_{\max}$  remains unknown, optimal measurement strategies are known for several other criteria [30, 33–35]. We proceed with a brief description of these strategies.

To begin with, consider a discrimination strategy that minimizes the error rate in identifying the detector states, subject to a *fixed rate of inconclusive outcomes*, namely the optimal FRIO measurement [28–30]. For equiprobable symmetric states, this strategy can be implemented through the following two-step process [36, 37]. First, an optimal separation map [31], characterized by a prescribed separation level  $\xi \in [0, 1]$ , reduces the overlaps between the input detector states  $\{|\alpha_{\ell}\rangle_d\}$  with the maximum success probability [38]

$$P_s(\xi) = \frac{n a_{\min}^2}{(1 - \xi) n a_{\min}^2 + \xi}, \quad (19)$$

where  $a_{\min} = \min\{a_k\}_{k \in \mathcal{I}}$ . In case of failure, the overlaps increase. Then, a minimum-error measurement discriminates the successful outputs, yielding conclusive outcomes (whether correct or not), while the failure outputs are discarded, yielding inconclusive outcomes with a fixed rate  $P_f(\xi) = 1 -$

$P_s(\xi)$ . This two-step process is represented by an  $(N + 1)$ -outcome POVM  $\mathbf{\Pi}_{\text{FRIO}} = \{\hat{\Pi}_0(\xi), \dots, \hat{\Pi}_{N-1}(\xi), \hat{\Pi}^f(\xi)\}$ . The elements  $\hat{\Pi}_j(\xi)$  and  $\hat{\Pi}^f(\xi)$ , associated with the conclusive and inconclusive outcomes, respectively, are given by [37, 38]

$$\hat{\Pi}_j(\xi) = |\phi_j(\xi)\rangle\langle\phi_j(\xi)|, \quad (20a)$$

$$\hat{\Pi}^f(\xi) = \frac{n}{N} \sum_{i,j=0}^{N-1} \langle u_i | u_j \rangle |\phi_i^f(\xi)\rangle\langle\phi_j^f(\xi)|, \quad (20b)$$

where

$$|u_j\rangle = \frac{1}{\sqrt{n}} \sum_{k \in \mathcal{I}} \omega^{jk} |k\rangle, \quad (21a)$$

$$|\phi_j(\xi)\rangle = \sqrt{P_s(\xi)} \sum_{k \in \mathcal{I}} g_k(\xi) \omega^{jk} |k\rangle, \quad (21b)$$

$$|\phi_j^f(\xi)\rangle = \sqrt{P_f(\xi)} \sum_{k \in \mathcal{I}} h_k \omega^{jk} |k\rangle, \quad (21c)$$

with  $g_k^2(\xi) = (1 - \xi + \xi/n a_k^2)/N$  and  $h_k^2 = (a_k^2 - a_{\min}^2)/(1 - n a_{\min}^2) N a_k^2$ .

The optimal FRIO measurement is a tunable strategy that balances the error and inconclusive rates within desired bounds, encompassing other fundamental strategies as special cases for extreme values of  $\xi$ . For  $\xi = 0$ , it reduces to the minimum-error (ME) measurement [33], described by the  $N$ -outcome POVM  $\mathbf{\Pi}_{\text{ME}} = \{\hat{\Pi}_j\}_{j=0}^{N-1}$ , where  $\hat{\Pi}_j = \hat{\Pi}_j(0) = \frac{n}{N} |u_j\rangle\langle u_j|$  [see Eqs. (21)]. For  $\xi = 1$ , it corresponds to the optimal unambiguous discrimination (UD) for linearly independent states ( $N = n$ ) [34], or to the optimal maximum-confidence (MC) measurement for linearly dependent states ( $N > n$ ) [35].

In the standard implementation of the optimal FRIO measurement, the failure output states are discarded, leading to inconclusive outcomes. However, when  $n > 2$ , these outputs often carry useful information about the inputs, opening the possibility for further discrimination attempts. Here, we consider the case in which the failure outputs are subsequently discriminated via a ME measurement, referring to this strategy as *concatenated FRIO*.<sup>1</sup> It is represented by a  $2N$ -outcome POVM  $\mathbf{\Pi}_{\text{CONC}} = \{\hat{\Pi}_j(\xi), \hat{\Pi}_j^f(\xi)\}_{j=0}^{N-1}$ , where  $\hat{\Pi}_j(\xi)$  and  $\hat{\Pi}_j^f(\xi)$  are the elements associated with a conclusive identification of the input state after successful and failed separations, respectively, which are given by [37]

$$\hat{\Pi}_j(\xi) = |\phi_j(\xi)\rangle\langle\phi_j(\xi)|, \quad (22a)$$

$$\hat{\Pi}_j^f(\xi) = |\phi_j^f(\xi)\rangle\langle\phi_j^f(\xi)|, \quad (22b)$$

<sup>1</sup> This is a slight abuse of language, since the “concatenated FRIO” does not produce inconclusive outcomes. However, we adopt this terminology throughout the article to distinguish it from “standard FRIO” and also because it effectively conveys the idea that the main strategy (optimal FRIO) is applied first; if it fails, a second strategy (ME) is then used to extract the remaining information.

with the states  $|\phi_j(\xi)\rangle$  and  $|\phi_j^f(\xi)\rangle$  defined in Eqs. (21).

Therefore, in our interferometric scenario, the acquisition of which-path knowledge—and its implications for duality relations—will be analyzed using different discrimination strategies determined by the value of  $\xi$ , and under both standard and concatenated measurement approaches.

### III. ENTROPIC WAVE-PARTICLE DUALITY RELATIONS

Just as visibility and distinguishability are constrained by a duality relation in two-path interferometers [see Eq. (2)], coherence and accessible information satisfy a similar relation, though not in quadratic form [17, 21]. To see this, we use the Holevo bound [39] along with Eqs. (11) and (13), obtaining

$$\mathcal{K}_{\max} \leq \frac{S(\hat{\rho}_d)}{\log_2 N} = \frac{H(\{a_k^2\})}{\log_2 N} = 1 - \mathcal{C}, \quad (23)$$

which implies  $\mathcal{C} + \mathcal{K}_{\max} \leq 1$ . Since the quanton state's coherence is fixed by the set of detector states, this entropic wave-particle duality relation is the tightest possible in  $N$ -path interferometers. When the which-path measurement  $\Pi$  does not attain the accessible path information, i.e.,  $\mathcal{K}(\Pi) \leq \mathcal{K}_{\max}$ , the relation becomes less tight and is given by

$$\mathcal{C} + \mathcal{K}(\Pi) \leq 1. \quad (24)$$

In this section, we derive duality relations of this form, based on the measurement strategies outlined in Sec. II D.

#### A. Duality relation for standard FRIQ measurement and limiting cases

For the optimal FRIQ measurement, the probabilities appearing in Eq. (17) depend on the separation parameter  $\xi$  and are computed using Eqs. (8), (11), and (19)-(21). The total probabilities of obtaining a conclusive and an inconclusive outcome are given by  $p_j(\xi) = \text{Tr}[\hat{\Pi}_j(\xi)\hat{\rho}_d] = P_s(\xi)/N$  and  $p_f(\xi) = \text{Tr}[\hat{\Pi}^f(\xi)\hat{\rho}_d] = P_f(\xi)$ , respectively. From Eq. (16), the conditional probability distributions corresponding to conclusive and inconclusive outcomes are, respectively,

$$p_{\ell|j}(\xi) = \left| \sum_{k \in \mathcal{I}} a_k g_k(\xi) \omega^{k(j-\ell)} \right|^2, \quad (25a)$$

$$p_{\ell|f} = \frac{1}{N}, \quad (25b)$$

where the latter represents a random guess of the detector state, and thus of the quanton's path. The distributions  $p_{\ell|j}(\xi)$  for different  $j$  are related by cyclic shifts in  $\ell$ , i.e.,  $p_{\ell|j}(\xi) = p_{\ell-j|0}(\xi)$ , where the subtraction  $\ell - j$  is modulo  $N$ . Since the Shannon entropy is invariant under cyclic permutation of the index  $\ell$ , it follows that  $H(\{p_{\ell|j}(\xi)\}) = H(\{p_{\ell|0}(\xi)\})$  for all  $j = 0, \dots, N-1$ . Thus, inserting these results into Eq. (17) yields the which-path knowledge:

$$\mathcal{K}(\Pi_{\text{FRIQ}}) = P_s(\xi) \tilde{\mathcal{H}}(\{p_{\ell|0}(\xi)\}), \quad (26)$$

where we introduced the shorthand notation

$$\tilde{\mathcal{H}}(\{x\}) := 1 - \frac{H(\{x\})}{\log_2 N} \quad (27)$$

for a quantity that will appear frequently, thereby enabling more compact and clearer expressions in what follows. Using Eq. (13), the corresponding duality relation is given by

$$\mathcal{C} + \mathcal{K}(\Pi_{\text{FRIQ}}) = \tilde{\mathcal{H}}(\{a_k^2\}) + P_s(\xi) \tilde{\mathcal{H}}(\{p_{\ell|0}(\xi)\}) \leq 1. \quad (28)$$

For all  $\xi \in [0, 1]$ , this relation is always saturated in the following two cases, which we refer to as trivial saturation points: when the detector states are orthogonal ( $a_k^2 = 1/N$  for all  $k$ ), in which case  $\mathcal{K}(\Pi_{\text{FRIQ}}) = 1$ , or when they are all identical, resulting in  $\mathcal{C} = 1$ . Later we will show that there also exist nontrivial saturation points in specific interferometric scenarios.

For a fixed set of detector states, specified by the coefficients  $\{a_k\}$ , the which-path knowledge in Eq. (26) is a strictly decreasing function of  $\xi$ ,<sup>2</sup> making the duality relation in Eq. (28) less tight as  $\xi$  increases. This is illustrated in the plot of  $\mathcal{C}$  versus  $\mathcal{K}(\Pi_{\text{FRIQ}})$  shown in Fig. 1, for a two-path interferometer and three values of the separation parameter. Therefore, the weakest bound occurs at  $\xi = 1$ , which corresponds to the optimal UD (or MC) strategy. For instance, when the detector states are linearly independent, we have  $p_{\ell|0}(1) = \delta_{\ell 0}$ , and the which-path knowledge reduces to  $\mathcal{K}(\Pi_{\text{UD}}) = P_s(1) = N a_{\min}^2$ , in agreement with Ref. [21]. In contrast, the tightest duality relation among those derived from the standard FRIQ measurement is achieved at  $\xi = 0$ , where the detector states are discriminated using the ME strategy. It is given by

$$\mathcal{C} + \mathcal{K}(\Pi_{\text{ME}}) = \tilde{\mathcal{H}}(\{a_k^2\}) + \tilde{\mathcal{H}}(\{p_{\ell|0}(0)\}) \leq 1. \quad (29)$$

The ME POVM for discriminating equiprobable symmetric states is given by  $\hat{\Pi}_j = \frac{n}{N} |u_j\rangle\langle u_j| = \hat{\Phi}^{-1/2} |\alpha_j\rangle\langle\alpha_j| \hat{\Phi}^{-1/2}$ , where  $\hat{\Phi} = \sum_{j=0}^{N-1} |\alpha_j\rangle\langle\alpha_j|$ . This measurement, known as the square-root measurement [40], has two important features regarding the maximization of the mutual information. First, it provides a close approximation to the accessible information when the states to be discriminated are equally likely and nearly orthogonal [41]. Second, it satisfies the necessary (but not sufficient) condition for attaining the accessible information [33]. Accordingly, the ME discrimination of the detector states yields an extremum—though not necessarily a maximum—of the which-path knowledge, and closely approximates  $\mathcal{K}_{\max}$  when  $d\langle\alpha_\ell|\alpha_{\ell'}\rangle_d \approx 0$  for all  $\ell \neq \ell'$ . The equality  $\mathcal{K}(\Pi_{\text{ME}}) = \mathcal{K}_{\max}$  always holds for two-path interferometers with pure detector states, as the optimal measurements for both criteria coincide [42]. For interferometers with  $N > 2$  paths, the equality holds only at the saturation points of the duality relation.

<sup>2</sup>  $P_s(\xi)$  and  $\tilde{\mathcal{H}}(\{p_{\ell|0}(\xi)\})$  are strictly decreasing and increasing functions of  $\xi$ , respectively, but the rate of decay of the former dominates the growth of the latter.

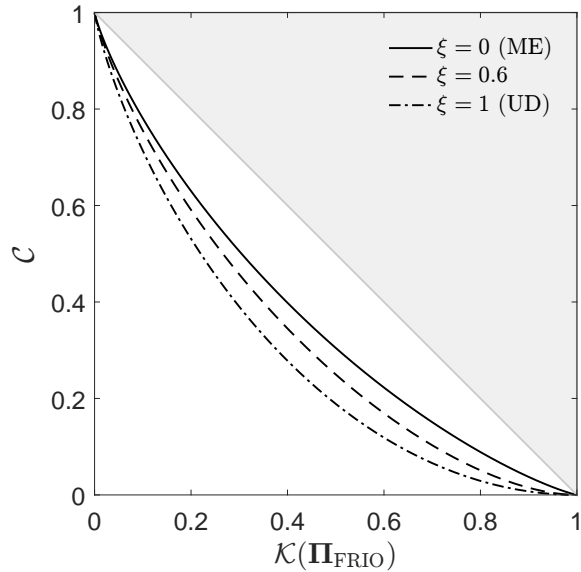


FIG. 1. Coherence vs which-path knowledge for uniform two-path interferometers with detector states discriminated via optimal FRIO measurement, using the separation parameter  $\xi = 0$  (solid line, ME measurement),  $\xi = 0.6$  (dashed line), and  $\xi = 1$  (dot-dashed line, optimal UD measurement). The shaded area is the region forbidden by the duality relation.

### B. Duality relation for concatenated FRIO measurement

Using the POVM defined in Eq. (22) and following the same steps as in the standard case, we compute the probabilities appearing in Eq. (17) for the concatenated FRIO measurement. The total probabilities of obtaining a conclusive outcome after successful and failed events are  $p_j(\xi) = P_s(\xi)/N$  and  $p_j^f(\xi) = P_f(\xi)/N$ , respectively. The corresponding conditional probability distributions  $p_{\ell|j}(\xi)$  and  $p_{\ell|j}^f$  are given by Eq. (25a) and

$$p_{\ell|j}^f = \left| \sum_{k \in \mathcal{I}} a_k h_k \omega^{k(j-\ell)} \right|^2, \quad (30)$$

respectively. Note that the distributions  $p_{\ell|j}^f$  do not depend on  $\xi$  and, like  $p_{\ell|j}(\xi)$ , are related by cyclic shifts in  $\ell$  for different  $j$ , i.e.,  $p_{\ell|j}^f = p_{\ell-j|0}^f$ . It follows that  $H(\{p_{\ell|j}^f\}) = H(\{p_{\ell|0}^f\})$  for all  $j = 0, \dots, N-1$ . Thus, inserting these results into Eq. (17) and using Eq. (26), we can write the which-path knowledge as

$$\mathcal{K}(\Pi_{\text{CONC}}) = \mathcal{K}(\Pi_{\text{FRIO}}) + P_f(\xi) \tilde{\mathcal{H}}(\{p_{\ell|0}^f\}), \quad (31)$$

which leads to the corresponding duality relation

$$\begin{aligned} \mathcal{C} + \mathcal{K}(\Pi_{\text{CONC}}) &= \tilde{\mathcal{H}}(\{a_k^2\}) + P_s(\xi) \tilde{\mathcal{H}}(\{p_{\ell|0}(\xi)\}) \\ &\quad + P_f(\xi) \tilde{\mathcal{H}}(\{p_{\ell|0}^f\}) \leq 1. \end{aligned} \quad (32)$$

Equation (31) make it evident that  $\mathcal{K}(\Pi_{\text{CONC}}) \geq \mathcal{K}(\Pi_{\text{FRIO}})$ . Moreover, as in the standard case,  $\mathcal{K}(\Pi_{\text{CONC}})$  is a strictly decreasing function of  $\xi$  for a fixed set of detector states.<sup>3</sup> As a consequence, we can establish the hierarchy  $\mathcal{K}(\Pi_{\text{FRIO}}) \leq \mathcal{K}(\Pi_{\text{CONC}}) \leq \mathcal{K}(\Pi_{\text{ME}}) \leq \mathcal{K}_{\text{max}}$ , which shows that the duality relation for the concatenated FRIO measurement is tighter than that of its standard counterpart [Eq. (28)], but still less tight than for the ME measurement [Eq. (29)]. Next, we will analyze and discuss the results presented in this section through numerical simulations.

### IV. COMPARATIVE ANALYSIS OF THE DUALITY RELATIONS VIA NUMERICAL SIMULATIONS

To assess the wave-particle duality relations derived above and compare their behavior under different measurement strategies, we carry out numerical simulations in MATLAB as follows. First, we set the number of paths in the interferometer ( $N$ ) and the dimension of the detector's Hilbert space ( $n$ ). Then, we generate a given number of random sets of detector states; for each set, we compute the quanton state's coherence using Eq. (13) and the which-path knowledge using either Eq. (26) or Eq. (31), for a fixed value of the parameter  $\xi$ . The obtained results will be displayed in scatter plots of  $\mathcal{C}$  versus  $\mathcal{K}(\Pi)$ . In all subsequent plots, the shaded area corresponds to the region forbidden by the duality relations [Eqs. (28), (29), and (32)].

#### A. Results for the ME measurement

Here, we consider detector states discriminated via ME measurement, i.e.,  $\xi = 0$ . Following the procedure described above, Fig. 2 shows the results for  $N = 3, 4, 5$ , and  $6$ , with  $n = N$  (orange dots). In all cases, the scatter plots exhibit the resulting  $(\mathcal{K}, \mathcal{C})$  points spanning a well-defined region—whose shape varies with  $N$ —within the bounds imposed by the duality relation. The boundaries of these regions feature cusps and inflection points. We observed empirically that these points correspond to specific sets of *uniform* detector states embedded in  $n$ -dimensional subspaces of the detector space, i.e., states with  $a_k = 1/n$  for all  $k \in \mathcal{I}$  [see, e.g., Eq. (21a)]. An indication of this correspondence is that the trivial saturation points  $(0, 1)$  and  $(1, 0)$ , which are cusps, occur for states of this form with  $n = 1$  and  $n = N$ , respectively.

To illustrate the observed correspondence, we first note that for each fixed integer  $n \leq N$ , there exist  $\binom{N}{n}$  distinct  $n$ -dimensional subspaces spanned by subsets of the orthonormal basis  $\{|k\rangle\}_{k=0}^{N-1}$ . Each subspace, in turn, supports a set of uniform symmetric states. To obtain the corresponding  $(\mathcal{K}, \mathcal{C})$

<sup>3</sup> Since the failure output states from the separation process are less distinguishable than the inputs, the entropy of  $\{p_{\ell|0}^f\}$  is high. Therefore, although the second term in  $\mathcal{K}(\Pi_{\text{CONC}})$  increases with  $\xi$ , this is not sufficient to offset the decay of  $\mathcal{K}(\Pi_{\text{FRIO}})$ .

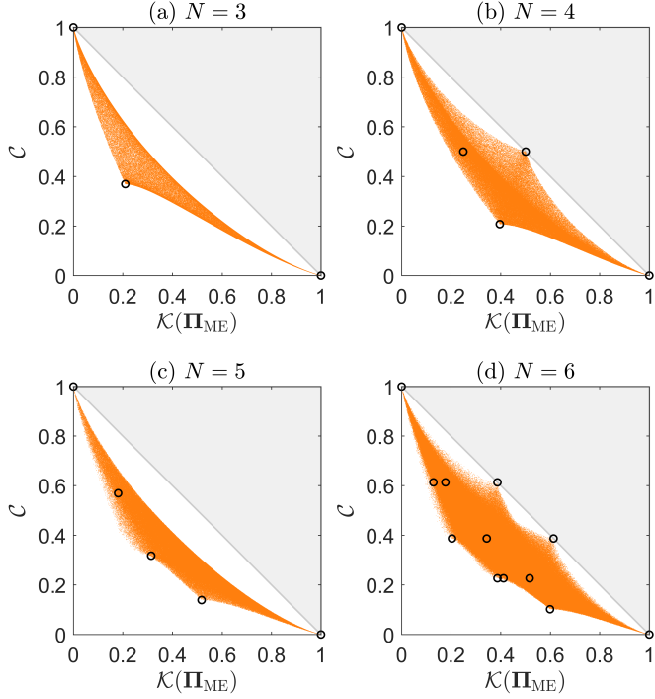


FIG. 2. Coherence vs which-path knowledge for uniform  $N$ -path interferometers with detector states discriminated via ME measurement. Orange dots: simulations with (a)  $10^5$ , (b)  $3 \times 10^5$ , (c)  $2.5 \times 10^5$ , and (d)  $3 \times 10^6$  randomly generated sets of  $N$ -dimensional detector states. Open black circles: simulations with all  $\binom{N}{n}$  sets of uniform  $n$ -dimensional detector states; sets yielding the same coherence correspond to a fixed value of  $n$ , ranging from  $n = 1$  ( $\mathcal{C} = 1$ ) to  $n = N$  ( $\mathcal{C} = 0$ ).

points, we generate all  $\binom{N}{n}$  such sets for  $n$  ranging from 1 to  $N$ , with each fixed  $n$  yielding  $\mathcal{C} = 1 - \log_2 n / \log_2 N$ , and then compute  $\mathcal{K}(\Pi_{ME})$ . The results are plotted as open black circles in Fig. 2. Among the sets with fixed  $n$ , many are physically equivalent (inequivalent), yielding the same (different)  $\mathcal{K}(\Pi_{ME})$  values and consequently superimposed (displaced) points. As we discuss below, the inequivalent sets are characterized by different structures of the support  $\mathcal{I}$  [see Eq. (4)], whereas equivalent sets share the same structure. The results in Fig. 2 clearly show that the cusps and inflection points of the boundaries arise from sets of uniform detector states.

In particular, for  $N = 4$  and  $N = 6$ , there are cusps on the saturation line beyond the trivial cases, indicating that the duality relation is also saturated at certain intermediate points. In Sec. V, we demonstrate that the relation in Eq. (29) is saturated at nontrivial  $(\mathcal{K}, \mathcal{C})$  points only for uniform detector states spanning an  $n$ -dimensional subspace, where  $n$  is a non-trivial divisor of  $N$  (i.e.,  $1 < n < N$ ), consistent with the results shown in Fig. 2. In addition, we determine the structure of the support underlying these states.

Still within the ME framework, in Fig. 3 we present results for a six-path interferometer with linearly dependent detector states spanning  $n$ -dimensional subspaces, with  $n$  ranging from 5 down to 2 (orange dots). The only trivial saturation point in this case is  $(0, 1)$ , as the detector states are never or-

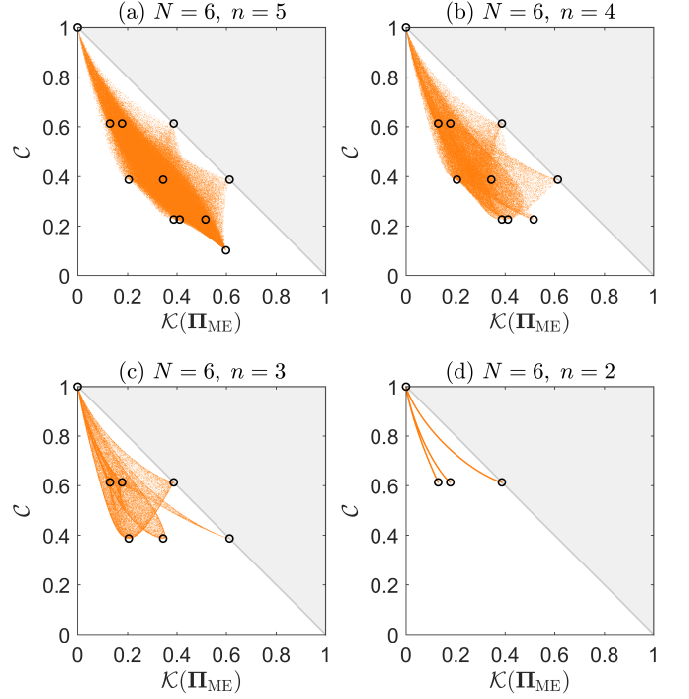


FIG. 3. Coherence vs which-path knowledge for uniform six-path interferometers with detector states discriminated via ME measurement. Orange dots: simulations with (a)  $3 \times 10^5$ , (b)  $10^5$ , (c)  $5 \times 10^4$ , and (d)  $10^4$  randomly generated sets of  $n$ -dimensional detector states. Open black circles: simulations with all  $\binom{N}{n'}$  sets of uniform  $n'$ -dimensional detector states; sets yielding the same coherence correspond to a fixed value of  $n'$ , ranging from  $n' = 1$  ( $\mathcal{C} = 1$ ) to  $n' = n$  ( $\mathcal{C} = 0$ ).

thogonal. Comparing with the plot in Fig. 2(d), we see that the region occupied by the  $(\mathcal{K}, \mathcal{C})$  points progressively decreases with  $n$ , reflecting the increasingly limited which-path knowledge. In Fig. 3, we also plot the  $(\mathcal{K}, \mathcal{C})$  points for all  $\binom{N}{n'}$  sets of uniform  $n'$ -dimensional detector states, with  $n'$  ranging from 1 to  $n$  (open black circles). These results show that, in the linearly dependent regime, the uniform  $n$ -dimensional states yield minima of coherence. However, while coherence is blind to the structure of the support [see Eq. (13)], which-path knowledge is sensitive to it [see Eqs. (25a) and (26)]. Consequently, we observe families of uniform states that, despite yielding the same coherence minima, provide different amounts of path knowledge when extracted via ME measurement.

To illustrate the role of the support structure on the (in)equivalence of the sets of uniform detector states and how it influences the distribution of the  $(\mathcal{K}, \mathcal{C})$  points, we examine the case  $n = 2$  shown in Fig. 3(d). In this scenario, three distinct curves emerge from  $(0, 1)$ . The simulations reveal that each curve, from left to right, corresponds to a specific structure of  $\mathcal{I}$ : unequally spaced nonadjacent ( $\mathcal{I} = \{0, 2\}$ ), unequally spaced adjacent ( $\mathcal{I} = \{0, 1\}$ ), and equally spaced ( $\mathcal{I} = \{0, 3\}$ ), including all their cyclic shifts. A deeper analysis of these aspects is provided in Sec. V.

## B. Results for the standard and concatenated FRIO measurements

We now assess the duality relations from Eqs. (28) and (32), where which-path knowledge is obtained through standard and concatenated FRIO measurements, respectively, using a fixed nonzero value of the separation parameter  $\xi$ . Again, we consider interferometers with  $N = 3, 4, 5$ , and 6 paths, where the quanton is coupled to an  $N$ -dimensional detector. Figure 4 displays plots of  $\mathcal{C}$  versus  $\mathcal{K}(\Pi_{\text{FRIO}})$  (orange dots, first and third rows) and  $\mathcal{C}$  versus  $\mathcal{K}(\Pi_{\text{CONC}})$  (green dots, second and fourth rows), with columns indicating the value of  $N$  and the upper (lower) two rows corresponding to  $\xi = 0.6$  ( $\xi = 1$ ). To facilitate comparison with the ME case, we also include the boundaries of the corresponding regions from the  $\mathcal{C}$ - $\mathcal{K}(\Pi_{\text{ME}})$  plots in Fig. 2, shown here as solid black lines.<sup>4</sup>

Taking the ME boundaries as a reference, the  $(\mathcal{K}, \mathcal{C})$  points for the standard FRIO measurement clearly span a much broader region for all values of  $N$  and  $\xi$ . Moreover, as  $\xi$  increases, the regions shift away from the saturation line, reflecting the reduced tightness of the duality relations, as discussed earlier. Since  $\mathcal{C}$  is independent of the discrimination strategy applied to the detector states, the observed broadening and leftward shift arise from a nonuniform reduction in which-path knowledge. These effects are mainly driven by the success probability of state separation, which modulates  $\mathcal{K}(\Pi_{\text{FRIO}})$  [see Eq. (26)]. For instance, when the detector states contain a very small coefficient  $a_{\min}$ ,  $P_s(\xi)$  [see Eq. (19)], and consequently  $\mathcal{K}(\Pi_{\text{FRIO}})$ , approach zero.

For the concatenated FRIO measurement, the results in Fig. 4 show that the regions spanned by the  $(\mathcal{K}, \mathcal{C})$  points are now more similar in shape and spatially closer to those of the ME case. Thus, compared to the standard FRIO, the regions narrow and shift rightward, approaching the saturation line.<sup>5</sup> These effects arise from a nonuniform increase in which-path knowledge, driven by the second term on the right-hand side of Eq. (31). As expected, the plots also show that the tightness of the duality relation decreases with increasing  $\xi$ .

Examining Fig. 4, we observe that the results for concatenated FRIO and ME measurements tend to become closer as  $\mathcal{C}$  increases or  $\xi$  decreases, scenarios in which the two strategies are more similar. Increased coherence is associated with reduced distinguishability of the detector states  $\{|\alpha_\ell\rangle_a\}$ . In this case, the separation stage succeeds with low probability  $P_s(\xi)$ , and the resulting failure states are discriminated via ME with high probability  $P_f(\xi) = 1 - P_s(\xi)$ . On the other hand, as  $\xi$  decreases, the input states are separated

with increasing success probability and undergo progressively smaller transformations before being discriminated via ME measurement.

In summary, the results expressed through the  $\mathcal{C}$ - $\mathcal{K}(\Pi)$  plots of Figs. 2, 3, and 4 illustrate the behaviors predicted by the duality relations derived in the previous section. They also reveal additional features that only became apparent through graphical analysis. In particular, we highlight the distinctive shapes of the  $(\mathcal{K}, \mathcal{C})$  point distributions, as well as the emergence of nontrivial saturation points, depending on the specific interferometric scenario. In the next section, we provide a rigorous analysis of the saturation behavior.

## V. ON THE SATURATION OF THE DUALITY RELATION

Here, we analyze the conditions under which the duality relation is saturated in our interferometric framework. We characterize the sets of detector states that lead to saturation (referred to as *saturating sets*) and contrast them with those that do not, before illustrating the results with explicit examples.

### A. Characterizing the saturating sets

For the duality relation of Eq. (29), where which-path knowledge is obtained via ME measurement, it can be readily shown that saturation occurs if and only if

$$H(\{a_k^2\}) + H(\{|\lambda_\ell|^2\}) = \log_2 N, \quad (33)$$

where

$$|\lambda_\ell|^2 := p_{\ell|0}(0) = \frac{1}{N} \left| \sum_{k \in \mathcal{I}} a_k \omega^{k\ell} \right|^2, \quad (34)$$

with  $p_{\ell|0}(0)$  obtained from Eq. (25a).

To determine the saturating sets, consider the vectors  $\vec{a} = \{a_k\}_{k \in \mathcal{I}} \in \mathbb{R}^N$  and  $\vec{\lambda} = \{\lambda_\ell\}_{\ell \in \mathcal{L}} \in \mathbb{C}^N$ . Here,  $\mathcal{I}$  and  $\mathcal{L}$  denote the supports of  $\vec{a}$  and  $\vec{\lambda}$ , respectively, and these vectors generate the corresponding probability distributions  $\{a_k^2\}$  and  $\{|\lambda_\ell|^2\}$ . From Eq. (34), we have  $\lambda_\ell = \frac{1}{\sqrt{N}} \sum_{k \in \mathcal{I}} a_k \omega^{k\ell}$ , so that  $\vec{\lambda}$  is the discrete Fourier transform (DFT) of  $\vec{a}$ . In this case, the discrete uncertainty principle states that [32]

$$|\mathcal{I}| \cdot |\mathcal{L}| \geq N \Rightarrow |\mathcal{L}| \geq \frac{N}{n}, \quad (35)$$

where we used  $|\mathcal{I}| = n$ . In other words, for two vectors of length  $N$  related by a DFT, if one has  $n$  nonzero entries, its DFT must have at least  $N/n$  nonzero entries. Hence, a vector concentrated on a few components in one domain must be spread over more components in the Fourier-conjugate domain, limiting simultaneous sparsity. For instance, if  $a_k = \delta_{kk'}$ , then  $|\lambda_\ell| = 1/\sqrt{N}$  for all  $\ell$ .

Let us first examine the conditions under which equality in Eq. (35) holds. As shown by Donoho and Stark [32], if  $N$

<sup>4</sup> These boundaries were obtained using the *boundary* function in MATLAB, which generates a tight polygon enclosing a set of points in 2D space. Note that when the point density near the boundary is low, the resulting shape becomes less smooth, as observed for  $N = 5$  and especially  $N = 6$ .

<sup>5</sup> For a fixed  $\xi > 0$ , the approach to the saturation line does not occur only for  $N = 3$ . In this case, the detector states at the upper boundary of the region take the form  $|\alpha_\ell\rangle = a_0|0\rangle + a_{\min}\omega^\ell|1\rangle + a_{\min}\omega^{2\ell}|2\rangle$ , leading to identical failure states in the separation stage ( $|\alpha_\ell\rangle \xrightarrow{\text{fail}} |0\rangle$  for all  $\ell$ ) and making concatenation ineffective.

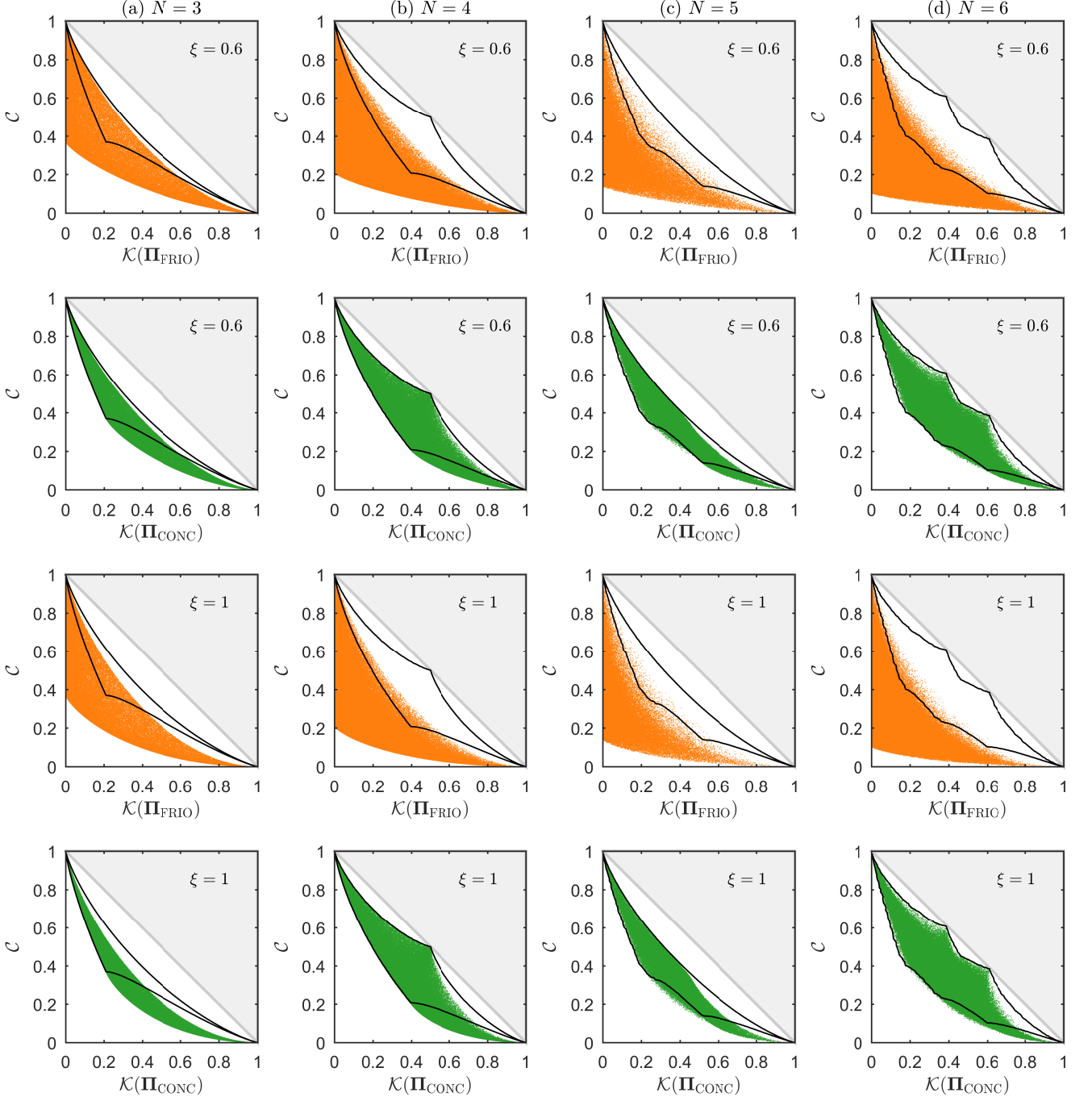


FIG. 4. Coherence vs which-path knowledge for uniform  $N$ -path interferometers with  $N$ -dimensional detector states discriminated via standard FRIO (first and third rows; orange dots) and concatenated FRIO (second and fourth rows; green dots), using the separation parameter  $\xi$  shown in the insets. The simulations were performed with (a)  $10^5$ , (b)  $3 \times 10^5$ , (c)  $10^5$ , and (d)  $10^6$  randomly generated sets of detector states. In each plot, the black solid line depicts the boundary of the corresponding region in the  $\mathcal{C}$  vs  $\mathcal{K}(\Pi_{\text{ME}})$  plots shown in Fig. 2.

admits the factorization  $N = nm$ , then the bound  $|\mathcal{L}| = m$  is attained by vectors  $\vec{a}$  given by

$$a_k = \begin{cases} \frac{1}{\sqrt{n}}, & k \in \mathcal{I}_{m,\tau} = \{\tau \oplus \kappa m \mid \kappa = 0, \dots, n-1\}, \\ 0, & \text{otherwise,} \end{cases} \quad (36)$$

where  $\tau \in \{0, \dots, m-1\}$  and  $\oplus$  denotes addition modulo  $N$ . The DFT of this vector is given by  $\lambda_\ell = \frac{\omega^{\tau\ell}}{\sqrt{Nn}} \sum_{\kappa=0}^{n-1} \omega^{\kappa m\ell}$ , where the sum is a geometric series with ratio  $r = \omega^{m\ell}$ . Since  $r^n = e^{2\pi i \ell} = 1$  for all  $\ell \in \{0, \dots, N-1\}$ , and  $r = 1$  if and only if  $\ell$  is a multiple of  $n$ , the sum equals  $n$  if  $\ell \in \{0, n, 2n, \dots, (m-1)n\}$ , and is zero otherwise. Substituting

this into  $\lambda_\ell$  and taking its modulus squared, we obtain

$$|\lambda_\ell|^2 = \begin{cases} \frac{n}{N}, & \ell \in \mathcal{L}_n = \{0, n, 2n, \dots, (m-1)n\}, \\ 0, & \text{otherwise.} \end{cases} \quad (37)$$

In this case, the entropies of the corresponding probability distributions take the values  $H(\{a_k^2\}) = \log_2 n$  and  $H(\{|\lambda_\ell|^2\}) = \log_2 N/n$ , whose sum satisfies the saturation condition of Eq. (33). Thus, from Eq. (36), we obtain saturating sets of detector states with the following form:

$$\begin{aligned} |u_\ell^{m,\tau}\rangle_d &= \frac{1}{\sqrt{n}} \sum_{k \in \mathcal{I}_{m,\tau}} \omega^{k\ell} |k\rangle_d \\ &= \frac{1}{\sqrt{n}} \sum_{\kappa=0}^{n-1} \nu^{\kappa\ell} |\tau \oplus \kappa m\rangle_d, \end{aligned} \quad (38)$$

where  $\nu = \exp(2\pi i/n)$ ; note that an irrelevant global phase factor,  $\omega^{\tau\ell}$ , has been omitted.

For any vector  $\vec{a}$  distinct from that of Eq. (36)—either uniform but supported on a set  $\mathcal{I} \neq \mathcal{I}_{m,\tau}$  or nonuniform—the discrete uncertainty principle in Eq. (35) implies that its DFT,  $\vec{\lambda}$ , is supported on a set of size  $|\mathcal{L}| > N/n$ . In such cases, the corresponding probability distribution  $\{|\lambda_\ell|^2\}$  spreads over more nonvanishing components, and the resulting increase in its entropy beyond  $\log_2(N/n)$  prevents the saturation condition in Eq. (33) from being fulfilled.

Therefore, in our interferometric framework, we conclude that the sets of detector states  $\{|u_\ell^{m,\tau}\rangle_d\}$  given by Eq. (38) constitute the only saturating sets. As these states are uniform, both the standard and concatenated FRIO strategies reduce to the ME measurement, since no further separation is possible. More importantly, as they span a subspace of dimension  $n = N/m$ , saturation can occur only when  $n$  divides  $N$ . Consequently, nontrivial saturation points exist exclusively in interferometers with a nonprime number of paths, located at  $\eta(N) - 2$  positions, where  $\eta(N)$  denotes the number of positive divisors of  $N$ , as illustrated in the examples of Fig. 2. To further exemplify this result, in Fig. 5 we show plots of  $\mathcal{C}$  versus  $\mathcal{K}(\Pi_{\text{ME}})$  for interferometers with  $N = 12$  and  $18$  paths, considering only uniform detector states. As already done in Sec. IV A, we compute the values of coherence and which-path knowledge for all  $\binom{N}{n}$  sets of uniform states, with  $n$  ranging from  $1$  to  $N$ . The obtained results confirm the above description.

The states  $|u_\ell^{m,\tau}\rangle_d$  in the saturating sets are characterized by an equally spaced support  $\mathcal{I}_{m,\tau}$  in the orthonormal basis  $\{|k\rangle_d\}_{k=0}^{N-1}$ , with the parameter  $m$  setting the spacing and  $\tau$  specifying the cyclic shift [see Eq. (36)]. Thus, for each  $n = N/m$ , there exist  $m$  physically equivalent saturating sets, each spanning the  $n$ -dimensional subspace generated by the basis vectors  $\{|\tau \oplus km\rangle_d\}_{k=0}^{n-1}$ . In Figs. 2(b), 2(d), and 5, the uniform detector states of dimension  $n = N/m$  that do not lead to saturation of the duality relation are supported on sets  $\mathcal{I}$  with unequally spaced structures. Next, we discuss why the support structure matters for achieving saturation.

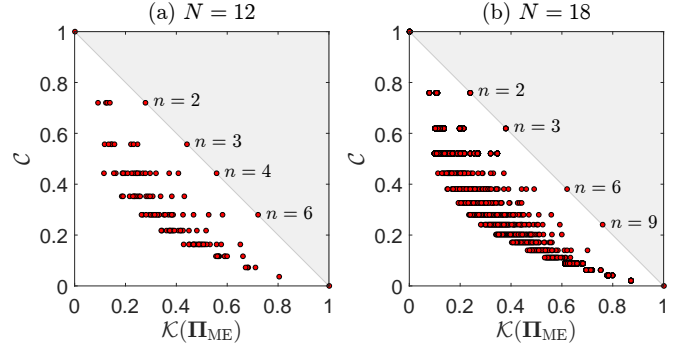


FIG. 5. Coherence vs which-path knowledge for uniform  $N$ -path interferometers with uniform  $n$ -dimensional detector states discriminated via ME measurement. All  $\binom{N}{n}$  sets of uniform detector states are generated, and those yielding the same coherence correspond to a fixed value of  $n$ , ranging from  $n = 1$  ( $\mathcal{C} = 1$ ) to  $n = N$  ( $\mathcal{C} = 0$ ). The insets show the values of  $n$  (beyond the trivial  $n = 1$  and  $n = N$ ) for which the duality relation of Eq. (29) is saturated.

## B. Role of the support structure in the quanton-detector correlations

The term  $\nu$  in Eq. (38) represents a primitive  $n$ th root of unity, implying that  $\nu^{jn} = 1$  for any integer  $j$  and  $\sum_{k=0}^{n-1} \nu^{k(\ell-\ell')} = n\delta_{\ell\ell'}$ . As a consequence,

$$|u_{\ell \oplus n}^{m,\tau}\rangle_d = |u_\ell^{m,\tau}\rangle_d \quad \text{and} \quad d\langle u_{\ell'}^{m,\tau} | u_\ell^{m,\tau} \rangle_d = \delta_{\ell\ell'}, \quad (39)$$

where  $\oplus$  here denotes addition modulo  $n$ . Thus, due to the equally spaced structure of their support, the states in the saturating sets repeat every  $n$  steps in the index  $\ell$  and form an orthonormal basis  $\{|u_\ell^{m,\tau}\rangle_d\}_{\ell=0}^{n-1}$  in the corresponding  $n$ -dimensional subspace. Using the periodicity of  $|u_\ell^{m,\tau}\rangle_d$  and reindexing  $\ell$  as  $\ell = l + jn$ , where  $l = 0, \dots, n-1$  and  $j = 0, \dots, m-1$ , the quanton-detector state [Eq. (7)] for the saturating sets can be expressed as

$$|\Psi\rangle = \frac{1}{\sqrt{n}} \sum_{l=0}^{n-1} |\psi_l\rangle_q |u_l^{m,\tau}\rangle_d, \quad (40)$$

where

$$|\psi_l\rangle_q = \frac{1}{\sqrt{m}} \sum_{j=0}^{m-1} |l + jn\rangle_q, \quad (41)$$

with  ${}_q\langle \psi_l | \psi_l \rangle_q = \delta_{ll'}$ . Thus, in the saturation scenario,  $|\Psi\rangle$  is a maximally entangled state of Schmidt rank  $n$ , establishing the maximum possible correlation between the quanton components  $|\psi_l\rangle_q$  and the detector states  $|u_l^{m,\tau}\rangle_d$ . Each  $|\psi_l\rangle_q$  corresponds to a uniform superposition of  $m$  path states equally spaced by  $n$ , and is correlated with  $|u_l^{m,\tau}\rangle_d$ , which belongs to an orthonormal set. Consequently, the ME measurement on the detector is a projective measurement in the basis  $\{|u_l^{m,\tau}\rangle_d\}_{l=0}^{n-1}$ , such that the identification of a detector state eliminates  $N - m$  of the  $N$  possible quanton path states. In this interferometric configuration, the resulting probability distribution  $\{|\lambda_\ell|^2\}$  is given by Eq. (37), which yields

the maximum which-path knowledge allowed by the quanton state's coherence, thus saturating the duality relation.

In contrast, for uniform detector states with unequally spaced support, the decomposition of  $|\Psi\rangle$  takes forms distinct from that in Eq. (40), leading to quanton-detector states that are not maximally entangled within their effective  $Nn$ -dimensional space. In such cases, the identification of a detector state eliminates fewer than  $N - m$  of the  $N$  possible quanton path states, thereby yielding less which-path knowledge than in the saturating case. Let us illustrate these aspects with the following example, introduced in Sec. IV A.

### 1. Six-path interferometers with two-dimensional detector states

In a uniform six-path interferometer with uniform two-dimensional detector states, the coherence of the quanton state is  $\mathcal{C} = 0.613$ . In this scenario, three inequivalent classes of detector-state sets have been identified [see Fig. 3(d)], each corresponding to a distinct support structure: equally spaced, unequally spaced adjacent, and unequally spaced nonadjacent. We start our analysis with the equally spaced support  $I_{3,0} = \{0, 3\}$ , corresponding to the saturating set defined in Eq. (38), in the subspace spanned by  $\{|0\rangle_d, |3\rangle_d\}$ . From Eqs. (40) and (41), the quanton-detector state takes the form

$$|\Psi\rangle = \frac{1}{\sqrt{2}} \left[ \left( \frac{|0\rangle_q + |2\rangle_q + |4\rangle_q}{\sqrt{3}} \right) |u_0^{3,0}\rangle_d + \left( \frac{|1\rangle_q + |3\rangle_q + |5\rangle_q}{\sqrt{3}} \right) |u_1^{3,0}\rangle_d \right], \quad (42)$$

where  $|u_l^{3,0}\rangle_d \propto |0\rangle_d + (-1)^l |3\rangle_d$ . Since  ${}_d\langle u_0^{3,0}|u_1^{3,0}\rangle_d = 0$ , the detector states are perfectly distinguishable; thus, identifying one of them eliminates three out of the six possible quanton path states. Using Eq. (34), we obtain the probability distribution  $(\frac{1}{3}, 0, \frac{1}{3}, 0, \frac{1}{3}, 0)$  for  $\{|\lambda_\ell|^2\}_{\ell=0}^5$ , in agreement with Eq. (37). This yields  $\mathcal{K}(\Pi_{\text{ME}}) = 0.387$ , and hence  $\mathcal{C} + \mathcal{K}(\Pi_{\text{ME}}) = 1$ . The same conclusions apply to  $I_{3,1} = \{1, 4\}$  and  $I_{3,2} = \{2, 5\}$ .

Now we consider the unequally spaced adjacent support  $I = \{0, 1\}$ , which corresponds to a nonsaturating set of detector states in the subspace spanned by  $\{|0\rangle_d, |1\rangle_d\}$ . In this case, the quanton-detector state reads

$$|\Psi\rangle = \frac{1}{\sqrt{6}} \left( |0\rangle_q |u_{0+}\rangle_d + |1\rangle_q |u_{1+}\rangle_d + |2\rangle_q |u_{2+}\rangle_d + |3\rangle_q |u_{0-}\rangle_d + |4\rangle_q |u_{1-}\rangle_d + |5\rangle_q |u_{2-}\rangle_d \right), \quad (43)$$

where  $|u_{l\pm}\rangle_d \propto |0\rangle_d \pm \omega^l |1\rangle_d$  (for  $l = 0, 1, 2$ ), so that  ${}_d\langle u_{l+}|u_{l-}\rangle_d = 0$  while  ${}_d\langle u_{l\pm}|u_{l'\pm}\rangle_d \neq 0$  for  $l \neq l'$ . Therefore, when the detector state is identified via ME measurement, e.g., as  $|u_{l+}\rangle_d$ , the quanton path state cannot be  $|l+3\rangle_q$ , eliminating only one of the six possible alternatives. This reduces the which-path knowledge in comparison to the previous case. From Eq. (34), we obtain the probability distribution  $(\frac{1}{3}, \frac{1}{4}, \frac{1}{12}, 0, \frac{1}{12}, \frac{1}{4})$  for  $\{|\lambda_\ell|^2\}_{\ell=0}^5$ , which yields  $\mathcal{K}(\Pi_{\text{ME}}) = 0.178$  and  $\mathcal{C} + \mathcal{K}(\Pi_{\text{ME}}) = 0.791$ . The

same conclusions hold for the other supports with this structure:  $I = \{1, 2\}, \{2, 3\}, \{3, 4\}, \{4, 5\}$ , and  $\{0, 5\}$ .

Finally, we examine the unequally spaced nonadjacent support  $I = \{0, 2\}$ , associated with a nonsaturating set of detector states in the subspace spanned by  $\{|0\rangle_d, |2\rangle_d\}$ . Here, the quanton-detector state is given by

$$|\Psi\rangle = \frac{1}{\sqrt{3}} \left[ \left( \frac{|0\rangle_q + |3\rangle_q}{\sqrt{2}} \right) |u_0\rangle_d + \left( \frac{|1\rangle_q + |4\rangle_q}{\sqrt{2}} \right) |u_1\rangle_d + \left( \frac{|2\rangle_q + |5\rangle_q}{\sqrt{2}} \right) |u_2\rangle_d \right], \quad (44)$$

where  $|u_l\rangle_d \propto |0\rangle_d + \omega^{2l} |2\rangle_d$  (for  $l = 0, 1, 2$ ), so that  ${}_d\langle u_l|u_{l'}\rangle_d \neq 0$  for  $l \neq l'$ . Thus, the identification of the detector state does not eliminate any of the quanton path states, reducing the which-path knowledge in comparison to both previous cases. In this case, the probability distribution  $\{|\lambda_\ell|^2\}_{\ell=0}^5$  is given by  $(\frac{1}{3}, \frac{1}{12}, \frac{1}{12}, \frac{1}{3}, \frac{1}{12}, \frac{1}{12})$ , which yields  $\mathcal{K}(\Pi_{\text{ME}}) = 0.129$  and  $\mathcal{C} + \mathcal{K}(\Pi_{\text{ME}}) = 0.742$ . The same conclusions hold for the other supports with this structure:  $I = \{0, 4\}, \{1, 3\}, \{1, 5\}, \{2, 4\}$ , and  $\{3, 5\}$ .

These examples highlight the role of the support structure from two complementary perspectives. First, the form of the quanton-detector state indicates how the correlations between the two systems are shaped by the support, providing intuition about the amount of available which-path information. Second, the resulting probability distribution  $\{|\lambda_\ell|^2\}$  shows a spread over an increasing number of nonvanishing components as the support departs from the equally spaced case, thus deviating from the saturating distribution given by Eq. (37). Taken together, these perspectives make clear why only uniform, symmetric detector states with equally spaced support form sets that lead to saturation of the duality relation in a uniform  $N$ -path interferometer.

## VI. CONCLUSION

In this work, we presented a quantitative study of wave-particle duality in multipath interferometers, addressing the case of  $N$  equally likely paths tagged by symmetric detector states. Within this interferometric framework, we established and provided detailed analysis of entropic duality relations between quantum coherence ( $\mathcal{C}$ ), characterized by the relative entropy of coherence of the quanton state, and which-path knowledge [ $\mathcal{K}(\Pi)$ ], quantified by the mutual information obtained through detector-state discrimination.

Our framework encompassed a wide variety of discrimination strategies, including those addressed in Refs. [16, 17, 21], as well as strategies not considered before. More importantly, it enabled the exact quantification of which-path knowledge, rather than relying only on upper bounds for  $\mathcal{K}(\Pi)$ , as done in those works. In this way, we provided a more precise assessment of the tightness of the duality relations according to the discrimination strategy employed. It was shown that the ME measurement yields the tightest bound, followed by the concatenated and standard FRIQ measurements, for which the tightness decreases as the separation parameter increases. In

this context,  $\mathcal{K}(\Pi)$  obtained via UD measurement yields the least tight relation, in contrast to the conclusion drawn from the upper bound in Ref. [16]. Moreover, our framework made it possible to identify the conditions under which the duality relations are saturated, explicitly revealing the role played by quanton-detector correlations in this phenomenon.

The discussion of wave-particle duality dates back almost a century, yet it remains relevant, particularly in the context of duality relations in multipath interferometers. Our findings offer novel insights into this topic and pave the way for experimental verification, as the discrimination strategies for symmetric states explored here have already been demonstrated in the laboratory [36, 43, 44].

## ACKNOWLEDGMENTS

This work was supported by CNPq INCT-IQ Grant No. 465469/2014-0 and CNPq Grants No. 422300/2021-7 and No. 303212/2022-5. L. F. M. acknowledges financial support from CAPES – Finance Code 001, and from the Project “Receptores não-convencionais em CV-QKD” supported by the EMBRAPII CIMATEC Competence Center in Quantum Technologies – Quantum Industrial Innovation (QuIIN), with financial resources from the PPI IoT/Manufatura 4.0 of the MCTI grant number 053/2023, signed with EMBRAPII. O. J. was supported by an internal grant from Universidad Mayor (PUENTE-2024-17).

- 
- [1] W. K. Wootters and W. H. Zurek, Complementarity in the double-slit experiment: Quantum nonseparability and a quantitative statement of Bohr’s principle, *Phys. Rev. D* **19**, 473 (1979).
- [2] H. Rauch and J. Summhammer, Static versus time-dependent absorption in neutron interferometry, *Phys. Lett. A* **104**, 44 (1984).
- [3] A. Zeilinger, Complementarity in neutron interferometry, *Physica B+C* **137**, 235 (1986).
- [4] P. Mittelstaedt, A. Prieur, and R. Schieder, Unsharp particle-wave duality in a photon split-beam experiment, *Found. Phys.* **17**, 891 (1987).
- [5] D. M. Greenberger and A. Yasin, Simultaneous wave and particle knowledge in a neutron interferometer, *Phys. Lett. A* **128**, 391 (1988).
- [6] L. Mandel, Coherence and indistinguishability, *Opt. Lett.* **16**, 1882 (1991).
- [7] G. Jaeger, A. Shimony, and L. Vaidman, Two interferometric complementarities, *Phys. Rev. A* **51**, 54 (1995).
- [8] B.-G. Englert, Fringe visibility and which-way information: An inequality, *Phys. Rev. Lett.* **77**, 2154 (1996).
- [9] P. D. D. Schwindt, P. G. Kwiat, and B.-G. Englert, Quantitative wave-particle duality and nonerasing quantum erasure, *Phys. Rev. A* **60**, 4285 (1999).
- [10] B.-G. Englert and J. A. Bergou, Quantitative quantum erasure, *Opt. Commun.* **179**, 337 (2000).
- [11] N. Bohr, in *Albert Einstein: Philosopher-Scientist*, edited by P. A. Schilpp (Library of Living Philosophers, Evanston, 1949) pp. 200–241.
- [12] S. Dürr, Quantitative wave-particle duality in multibeam interferometers, *Phys. Rev. A* **64**, 042113 (2001).
- [13] G. Bimonte and R. Musto, Comment on “Quantitative wave-particle duality in multibeam interferometers”, *Phys. Rev. A* **67**, 066101 (2003).
- [14] G. Bimonte and R. Musto, On interferometric duality in multibeam experiments, *J. Phys. A* **36**, 11481 (2003).
- [15] B.-G. Englert, D. Kaszlikowski, L. C. Kwek, and W. H. Chee, Wave-particle duality in multi-path interferometers: General concepts and three-path interferometers, *Int. J. Quantum Inf.* **06**, 129 (2008).
- [16] M. N. Bera, T. Qureshi, M. A. Siddiqui, and A. K. Pati, Duality of quantum coherence and path distinguishability, *Phys. Rev. A* **92**, 012118 (2015).
- [17] E. Bagan, J. A. Bergou, S. S. Cottrell, and M. Hillery, Relations between coherence and path information, *Phys. Rev. Lett.* **116**, 160406 (2016).
- [18] T. Qureshi and M. A. Siddiqui, Wave-particle duality in  $N$ -path interference, *Ann. Phys.* **385**, 598 (2017).
- [19] T. Qureshi, Interference visibility and wave-particle duality in multipath interference, *Phys. Rev. A* **100**, 042105 (2019).
- [20] P. Roy and T. Qureshi, Path predictability and quantum coherence in multi-slit interference, *Phys. Scr.* **94**, 095004 (2019).
- [21] E. Bagan, J. A. Bergou, and M. Hillery, Wave-particle-duality relations based on entropic bounds for which-way information, *Phys. Rev. A* **102**, 022224 (2020).
- [22] X. Lü, Quantitative wave-particle duality as quantum state discrimination, *Phys. Rev. A* **102**, 022201 (2020).
- [23] M. L. W. Basso, D. S. S. Chrysostemos, and J. Maziero, Quantitative wave-particle duality relations from the density matrix properties, *Quantum Inf. Process.* **19**, 254 (2020).
- [24] T. Baumgratz, M. Cramer, and M. Plenio, Quantifying coherence, *Phys. Rev. Lett.* **113**, 140401 (2013).
- [25] A.Chefles, Quantum state discrimination, *Contemp. Phys.* **41**, 401 (2000).
- [26] S. M. Barnett and S. Croke, Quantum state discrimination, *Adv. Opt. Photon.* **1**, 238 (2009).
- [27] J. A. Bergou, Discrimination of quantum states, *J. Mod. Opt.* **57**, 160 (2010).
- [28] A. Chefles and S. M. Barnett, Strategies for discriminating between non-orthogonal quantum states, *J. Mod. Opt.* **45**, 1295 (1998).
- [29] C.-W. Zhang, C.-F. Li, and G.-C. Guo, General strategies for discrimination of quantum states, *Phys. Lett. A* **261**, 25 (1999).
- [30] E. Bagan, R. Muñoz Tapia, G. A. Olivares-Rentería, and J. A. Bergou, Optimal discrimination of quantum states with a fixed rate of inconclusive outcomes, *Phys. Rev. A* **86**, 040303 (2012).
- [31] A. Chefles and S. M. Barnett, Quantum state separation, unambiguous discrimination and exact cloning, *J. Phys. A* **31**, 10097 (1998).
- [32] D. L. Donoho and P. B. Stark, Uncertainty principles and signal recovery, *SIAM J. Appl. Math.* **49**, 906 (1989).
- [33] M. Ban, K. Kurokawa, R. Momose, and O. Hirota, Optimum measurements for discrimination among symmetric quantum states and parameter estimation, *Int. J. Theor. Phys.* **36**, 1269 (1997).
- [34] A. Chefles and S. M. Barnett, Optimum unambiguous discrimination between linearly independent symmetric states, *Phys. Lett. A* **250**, 223 (1998).
- [35] O. Jiménez, M. A. Solís-Prosser, A. Delgado, and L. Neves, Maximum-confidence discrimination among symmetric qudit

- states, *Phys. Rev. A* **84**, 062315 (2011).
- [36] L. F. Melo, M. A. Solís-Prosser, O. Jiménez, A. Delgado, and L. Neves, Experimental optimal discrimination of  $N$  states of a qubit with fixed rates of inconclusive outcomes, *Phys. Rev. Res.* **5**, 043149 (2023).
- [37] L. F. Melo, O. Jiménez, and L. Neves, Coherence based on positive operator-valued measures for standard and concatenated quantum state discrimination with inconclusive results, *Phys. Rev. A* **111**, 012403 (2025).
- [38] M. A. Solís-Prosser, A. Delgado, O. Jiménez, and L. Neves, Parametric separation of symmetric pure quantum states, *Phys. Rev. A* **93**, 012337 (2016).
- [39] M. A. Nielsen and I. L. Chuang, *Quantum Computation and Quantum Information* (Cambridge University Press, Cambridge, 2000).
- [40] P. Hausladen, R. Jozsa, B. Schumacher, M. Westmoreland, and W. K. Wootters, Classical information capacity of a quantum channel, *Phys. Rev. A* **54**, 1869 (1996).
- [41] P. Hausladen and W. K. W. and, A ‘pretty good’ measurement for distinguishing quantum states, *J. Mod. Opt.* **41**, 2385 (1994).
- [42] A. Varga, P. Adam, and J. A. Bergou, Maximum information measurement for qubit states, *Sci. Rep.* **14**, 11888 (2024).
- [43] M. A. Solís-Prosser, M. F. Fernandes, O. Jiménez, A. Delgado, and L. Neves, Experimental minimum-error quantum-state discrimination in high dimensions, *Phys. Rev. Lett.* **118**, 100501 (2017).
- [44] M. A. Solís-Prosser, O. Jiménez, A. Delgado, and L. Neves, Enhanced discrimination of high-dimensional quantum states by concatenated optimal measurement strategies, *Quantum Sci. Technol.* **7**, 015017 (2022).